J Fluoresc (2009) 19:141–149
DOI 10.1007/s10895-008-0395-1

ORIGINAL PAPER

PARAFAC Analysis of the Quenching of EEM of Fluorescence of Glutathione Capped CdTe Quantum Dots by Pb(II)

Helena Gonçalves · Conceição Mendonça · Joaquim C. G. Esteves da Silva

Received: 12 May 2008 / Accepted: 20 June 2008 / Published online: 15 July 2008

Abstract Glutathione capped CdTe quantum dots (QD) were synthesised using a simple experimental procedure and two samples were subjected of study (QD_{550} and QD_{600}). The maximum of the excitation and emission spectra and the emission full width of half maximum of these two QD were: QD_{550}, 307, 550 and 37 nm; QD_{600}, 307, 600 and 39 nm. The steady state fluorescence properties of the two QD undergo variation when the pH of the aqueous solution is varied and are characterised by different apparent p*K*a: QD_{550}, 5.2±0.1; QD_{600}, 6.3±0.3. The fluorescence intensity of the QD_{550} is markedly quenched by the presence of micromolar quantities of Pb(II) ion (Stern–Volmer constant of about 7×10^5 M^{-1}). PARAFAC analysis of the excitation emission matrices (EEM) of QD_{550} acquired as function of the Pb(II) ion showed that only one linearly independent component describes the quenching of the QD_{550} by the Pb(II) ion allowing robust estimation of the excitation and emission spectra and of the quenching profiles.

Keywords Quantum dots · Glutathione · Pb(II) ion · Quenching of fluorescence · EEM · PARAFAC

Introduction

Quantum dots (QDs) are gaining a great scientific interest due to their tunable luminescent properties [1–3]. Also, by modifying the surface of QDs with hydrophilic capping ligands provides increased solubility and stability in water [4–6]. Usually one end of these hydrophilic capping ligands contains a thio group that binds with the QDs surface and the other, a polar end, makes them water soluble [4–6].

Glutathione (GSH) has been used as QDs stabilizer resulting in QDs with high photostability and quantum yield at room temperature in water [7–12]. The biological role of GSH is well known, for example as a free radical scavenger, amino acid transport, detoxification of xenobiotics, maintenance of protein redox state, neuromodulation and neurotransmission [7, 11, 12]. These GSH stabilized QDs can be used as biomarkers by themselves [9, 12] or when coated with bioprobes, like for example, streptavidin [8]. Also, taking into consideration the high affinity of GSH towards metal ions, QDs sensible to Pb(II) ion were developed [11].

Analytical applications of water soluble QDs for chemical species identification based on luminescence measurements have been proposed [11–22], either based on the enhancement or quenching of fluorescence. Although fluorescence is intrinsically a second-order method because it is able to generate an excitation emission matrix (EEM) of data points per sample [23, 24], the analytical methodologies that are being proposed are based on a single measurement—one fluorescence intensity for a pair of excitation and emission wavelengths. Moreover, if EEM are acquired as function of another variable, like for example the concentration of a chemical species that provokes variation on the fluorescence of the fluorophores present in the sample, a third-order method is obtained. One advantage of intrinsically tri-linear third-order data is that the profiles in each order can be determined uniquely for each species in the sample [24–27]. EEM has an intrinsically tri-linear structure and, consequently, have great potential for unique and robust decomposition [24–27].

The first application to chemical analysis of the 'unique decomposition property' was in the analysis of mixtures of

H. Gonçalves · C. Mendonça · J. C. G. Esteves da Silva (✉)
Centro de Investigação em Química, Departamento de Química,
Faculdade de Ciências da Universidade do Porto,
Rua Campo Alegre 687,
4169-007 Porto, Portugal
e-mail: jcsilva@fc.up.pt

aromatic hydrocarbons by molecular fluorescence spectroscopy coupled to liquid chromatography [28]. Since this first application, the potential of analyzing fluorescent three-way data matrices has been increasingly recognized [29–42]. PARAFAC (parallel factor analysis) [25–27] is a chemometric multi-way decomposition method particularly suitable for the analysis of EEM data because their model formulation are similar [26].

In this paper a simple synthesis of GSH capped CdTe QDs is described and two different size samples are characterized for the pH dependence and presence of Pb(II) ion on their steady state fluorescence. The quenching of the fluorescence of the GSH capped CdTe QDs is monitored by EEM. The structure of sets of EEM obtained as function of Pb(II) concentration will be analyzed by PARAFAC and the intrinsic quenching model calculated together with the excitation and emission spectra and the quenching profiles.

Theory: EEM and PARAFAC

The intensity of fluorescence emitted by a fluorophore is related to the excitation and emission wavelength and its concentration. An EEM contains all the steady state fluorescence features of a fluorophore and the fluorescence intensity at a particular pair of excitation and emission wavelengths. If several EEM are obtained for several samples containing different concentrations of the fluorophores (Fl—number of different fluorophores) a three-way matrix **F** is obtained, with elements f_{ijk} (fluorescence intensity of sample i at emission wavelength j and excitation wavelength k) given by:

$$f_{ijk} = \sum_{n=1}^{\mathrm{Fl}} c_{in}\mathrm{ex}_{jn}\mathrm{em}_{kn} + e_{ijk} \tag{1}$$

where c_{in} is the concentration of the n fluorophore in the i sample, ex_{jn} and em_{kn} are the excitation and emission spectra vectors of the n fluorophore and e_{ijk} is the residual error; the subscripts i and j correspond to the i^{th} excitation and j^{th} emission wavelengths, respectively.

The PARAFAC model of a three-way tri-linear data structure $X(i\times j\times k)$ with elements x_{ijk} corresponds to the product of three matrices $\mathbf{A}(i\times n)$, $\mathbf{B}(j\times n)$ and $\mathbf{D}(k\times n)$ plus the matrix of error $(E(i\times j\times k))$. Each element x_{ijk} can be calculated by:

$$x_{ijk} = \sum_{n=1}^{\mathrm{Fl}} a_{in}b_{jn}d_{kn} + e_{ijk} \tag{2}$$

where a_{in}, b_{jnkn} and e_{ijk} are respectively the elements of the **A**, **B**, **D** and **E** matrices. After selecting the number of components for the model, the three basic unknown matrices **A**, **B** and **C** are calculated by an iterative alternating least squares method without any restrictions. If the EEM follows a trilinear model (number of components equals the number of fluorophores) described in Eq. 1 then the PARAFAC solution (a, b and d) should be equivalent to the physico-chemical quantities (c, ex and em).

The results obtained from the different PARAFAC models were compared using the model fit [Fit (%)] defined by Eq. 3 [43]:

$$\mathrm{Fit}\ (\%) = 100 \times \left(1 - \sqrt{\frac{\sum_{i=1}^{I}\sum_{j=1}^{J}\sum_{k=1}^{K}\left(f_{ijk} - x_{ijk}\right)^2}{\sum_{i=1}^{I}\sum_{j=1}^{J}\sum_{k=1}^{K}\left(f_{ijk}\right)^2}}\right) \tag{3}$$

Also, the results obtained with PARAFAC models are assessed using the corcondia (core consistency) test defined by Eq. 4 [43]:

$$\mathrm{Corcondia}\ (\%) = 100 \times \left(1 - \frac{\sum_{d=1}^{N}\sum_{e=1}^{N}\sum_{f=1}^{N}\left(g_{def} - t_{def}\right)^2}{\sum_{d=1}^{N}\sum_{e=1}^{N}\sum_{f=1}^{N}\left(t_{def}\right)^2}\right) \tag{4}$$

In this equation g_{efg} and t_{efg} denote the elements of the calculated core and of the intrinsic super-diagonal core, respectively, and N the number of components of the model. If they are equal, the core consistency is perfect and has a value of unity (100%). Models with a corcondia value significantly lower than 100% should not be considered.

Experimental section

Reagents

Reagents and the respective percentages of purity were the following: tellurium powder (99.997%); cadmium chloride (99.99%); sodium tetrahydroborate (96%); L-GSH reduced (Sigma, minimum 99%). Deionised and deoxygenated water was used during the whole synthesis. Water deoxygenating was accomplished by boiling followed by cooling under nitrogen. An inert nitrogen atmosphere was maintained during all the synthesis. Standard 0.1 M aqueous solutions of Pb(II) nitrate was used. Rigorous dilution of this standard was obtained in the concentration range 1×10^{-7} and up to 1×10^{-5} M. Deionised water with resistivity higher than 4 MΩ/cm was used.

Synthesis of CdTe QD

All the synthesis of QD was based on that previously described [44–46] with the following particular characteristics: (1) 50 mg of sodium tetrahydroborate were mixed with 2 ml of water followed by 75 mg of tellurium—this

solution was left to stabilize for about 24 h; this solution was carefully decanted into 100 ml of water; (2) 230 mg of cadmium chloride was dissolved in 400 ml of water and mixed with 863 mg of GSH—the pH of this solution was rigorously fixed to 6.5 by the addition of sodium hydroxide 10 or 0.1 M; (3) The tellurium solution was transferred quickly and vigorously into the cadmium solution and the mixture were refluxed up to 8 h. Two samples of QD (named QD raw solutions) were removed when the emission wavelength reached about 550 (QD_{550}) and 600 nm (QD_{600}) for analysis and kept in the freeze at 5 °C.

Two strategies were used for QDs purification:

1. QDs raw solutions were dialyzed for 48 h against deionised water using a MW CO 12,000–14,000 Da dialysis tube from Medicell International. As the salt concentration decreases the QDs coagulate and precipitated (the first to precipitate was QD_{600}, followed by QD_{550}). The QDs suspension were freezed and lyophilized.
2. QDs were precipitated by mixing the raw solution with an equal volume of 2-propanol. The precipitated QD were centrifuged, washed with water without shaking and redissolved in 10 mM Hepes pH=7.5.

Acid-base and Pb(II) titrations

A diluted solution of each QD was prepared in a proportion of 1:25 ml in water. The pH of this diluted solution was reversibly varied in the range 4 to 10 with sodium hydroxide (0.1 M) and hydrogen chloride (0.1 M). Rigorous amounts (from 10 to 500 μl) of a standard 0.001 M Pb(II) ion solution were added to 50.00 ml of the QD solutions in Hepes pH=7.5—the concentration of Pb(II) ion ranged from 0 to 1×10^{-5} M.

Instrumentation

Scanning Electron Microscopy (SEM) and Energy dispersive X-ray (EDS) analysis of the three purified QDs were done on a FEI Quanta 400FEG/EDAX Genesis X4M High Resolution Scanning Electronic Microscope.

A Spex 3D Spectrofluorimeter with a 75 W xenon lamp and a CCD detector was used. Raw EEM were acquired in an excitation wavelength range from 199.4 to 672.8 nm (213 data points), and in an emission wavelength range from 250 to 710 nm (250 data points) using 0.05 mm slits and 3 s integration time.

Chemometric analysis

For chemometric analysis raw EEM were reduced to an excitation wavelength range from 199.4 to 396.4 nm (90 data points) and an emission wavelength range from 511 to 635 nm (60 data points). Experimental data matrices were arranged as a three dimensional array [number of Pb(II) concentrations × emission (nm) × excitation (nm)]—a typical dimension was (6, 60, 90).

All routines employed to carry out the calculations described in this paper were written in MATLAB version 7.5.0.342. The used PARAFAC code was available from http://www.models.kvl.dk/source/nwaytoolbox/.

Results and discussion

QDs properties

Figure 1 shows the evolution of the maximum of the emission spectra (Fig. 1a) and of the emission intensity (Fig. 1b) of the synthesized QD as function of the reaction time. The analysis of these figures show that the size of the QD increases with the reaction time as a result of the decrease of the carrier's confinement energy with the correspondent increase of the emission wavelength. Also, after 3 h of reaction time, the fluorescence intensity starts to

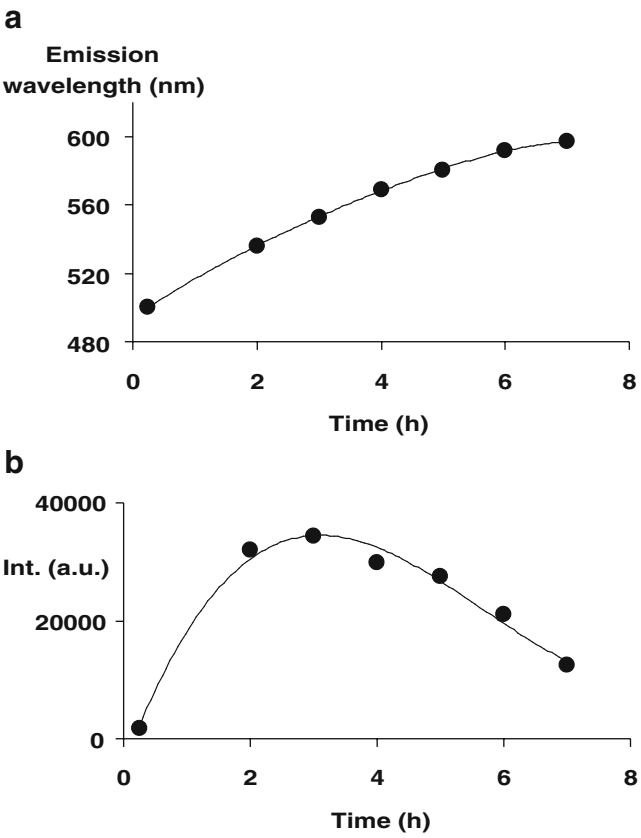

Fig. 1 Variation of the maximum of the emission spectra (**a**) and fluorescence intensity (**b**) of QD as function of the reaction time (excitation at about 435 nm)

decrease as consequence of the decrease of the quantum confinement. Under the experimental conditions used in this work GSH capped CdTe QD with maximum fluorescence intensity emit at about 550 nm (QD_{550}). Besides QD_{550} another sample was taken apart for detailed study after 7 h reaction time which has an emission maximum at about 600 nm (QD_{600}).

Figure 2 shows the SEM and EDS spectra of the dialyzed QD_{550}. SEM analysis of the coagulated QD shows that the dimension of QD_{550} is about 34±5 nm (Fig. 2a) and larger particles are also observed where the individual QD can be detected (Fig. 2b). Also, the EDS analysis (Fig. 2c) confirms that the synthesized QD are indeed GSH capped CdTe. The SEM analysis of the dialyzed QD_{600} could not detect individual but only large size particles (coagulated) QD.

Table 1 presents the steady state fluorescence properties of the QD_{550} and QD_{600}. The analysis of this table shows that besides a marked variation of the emission wavelength with the reaction time both the maximum excitation and the emission full width of half maximum (fwhm) of QD_{550} and QD_{600} show variation respectively, 351 and 367 nm and 62 and 49 nm.

The synthesized GSH capped QD are similar to other GSH capped QD, namely: CdSe QD—emission maximum= 533 nm and fwhm=49 nm [8]; CdTe QD—emission range=

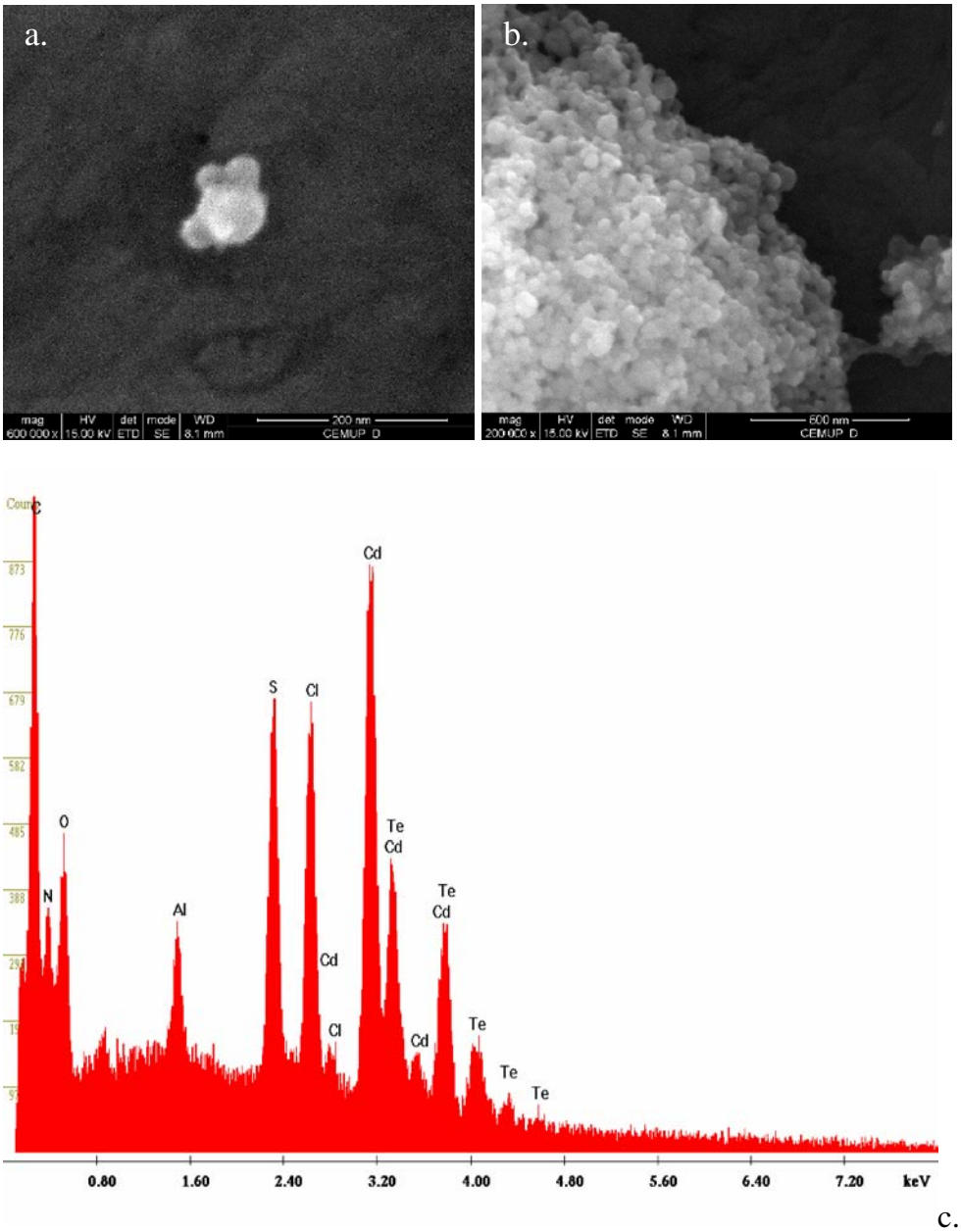

Fig. 2 SEM (**a**, **b**) photographs and EDS spectra (**c**) of the coagulated QD_{550}

Table 1 Photophysical and acid–base properties of the glutathione capped CdTe QD

Property	QD_{550}	QD_{600}
Excitation wavelength	351 nm (28,490 cm^{-1})	367 nm (27,248 cm^{-1})
Emission wavelength	550 nm (18,182 cm^{-1})	600 nm (16,667 cm^{-1})
fwhm	62 nm (20 eV)	49 nm (25 eV)
pH sensitivity range (ΔpH)	4.5–6.5	5.7–8.0
Variation of the emission wavelength with the pH ($\Delta\lambda_{acid/base}$)	18 nm (69 eV)	22 nm (56 eV)
pH sensitivity [$\Delta\lambda_{acid/base}/\Delta pH$ (nm^{-1})]	7.8	11
p*K*a	5.2±0.1	6.3±0.3

510 to 630 nm [9]; CdTe QD—emission maximum=529 nm [11]; ZnCdSe QD—emission maximum=469 nm [11].

pH effect on the QDs fluorescence properties

Varying the pH of the QD aqueous solution affects both the maximum emission wavelength and fluorescence intensity (Figs. 3 and 4). Both QD samples exhibited similar behaviour as function of the pH, i.e., the fluorescence intensity decreases and the maximum emission wavelength is shift towards longer wavelengths as the pH is decreased.

The variation of the emission wavelength with pH is shown in Fig. 4. The analysis of this figure shows that although the variation trend is similar the pH range where it occurs is different for both QD, demonstrating that they have different apparent acid–base properties (Table 1)—the higher the size of the QD more basic they become. Also, the variation interval of the maximum emission wavelength with the pH ($\Delta\lambda_{acid/base}$) increases with the size of the QD (QD_{550}, 18 nm; QD_{600}, 22 nm), revealing a higher degree of heterogeneity of the QD, i.e. a different number of GSH molecules capping the QDs. The relatively sensitivity of each QDs to the pH variation ($\Delta\lambda_{acid/base}/\Delta pH$) is also different: QD_{550}, 8 nm^{-1}; QD_{600}, 11 nm^{-1}. From the fitting of the maximum emission wavelength variation to Henderson–Hasselbalch type equation [47] the apparent p*K*a of both QD is 5.2±0.1 (QD_{550}) and 6.3±0.3 (QD_{600}).

This study shows that any analytical application of QD must be performed under constant pH. Also, if one is interested in pH measurement, alone or coupled to any other measurement, these quantum dots have high analytical potential as wavelength encoded pH sensors.

PARAFAC analysis of the quenching induced by Pb(II) ions

The presence of micromolar concentrations of Pb(II) in the QD solutions at pH=7.5 provoked marked quenching of the fluorescence of QD_{550} but almost no quenching on the fluorescence of QD_{600}. Only the interaction of QD_{550} with Pb(II) was subjected of study. Figure 5 shows typical EEM of the QD_{550} in the presence of different concentrations of Pb(II).

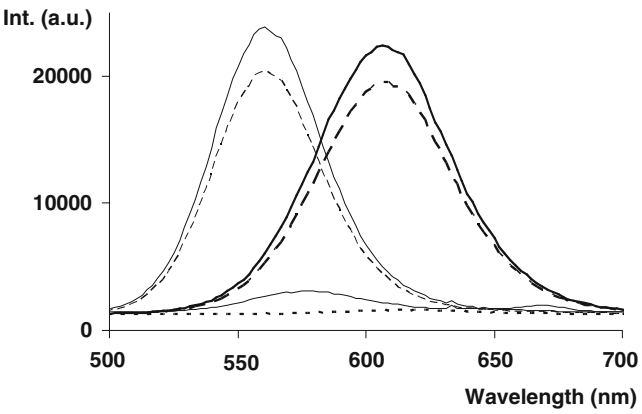

Fig. 3 Emission spectra of QD_{550} (*thin solid line*) and QD_{600} (*thick solid line*): pH=3 (*dotted line*); pH=7 (*solid line*); pH=11 (*dashed line*)

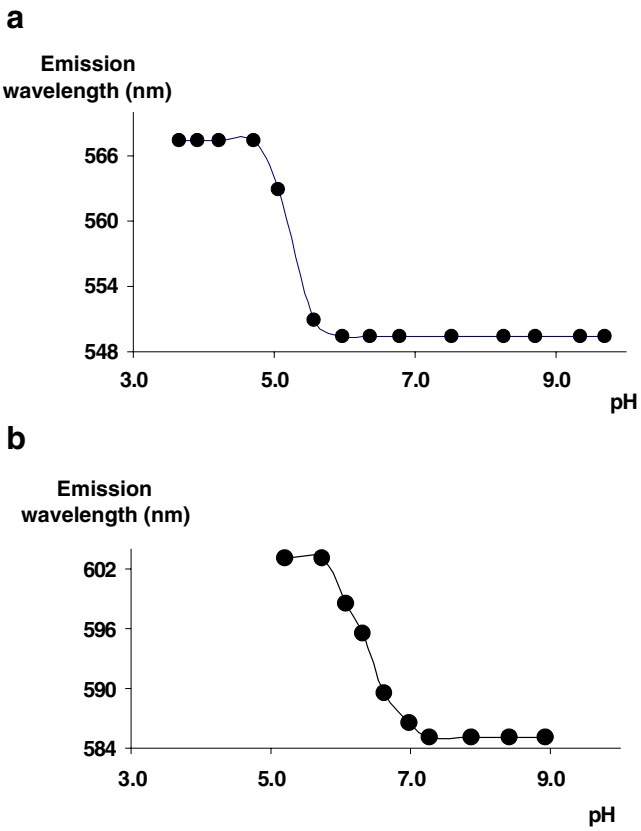

Fig. 4 Variation of the maximum emission wavelength with the solution pH for QD_{550} (**a**) and QD_{600} (**b**)

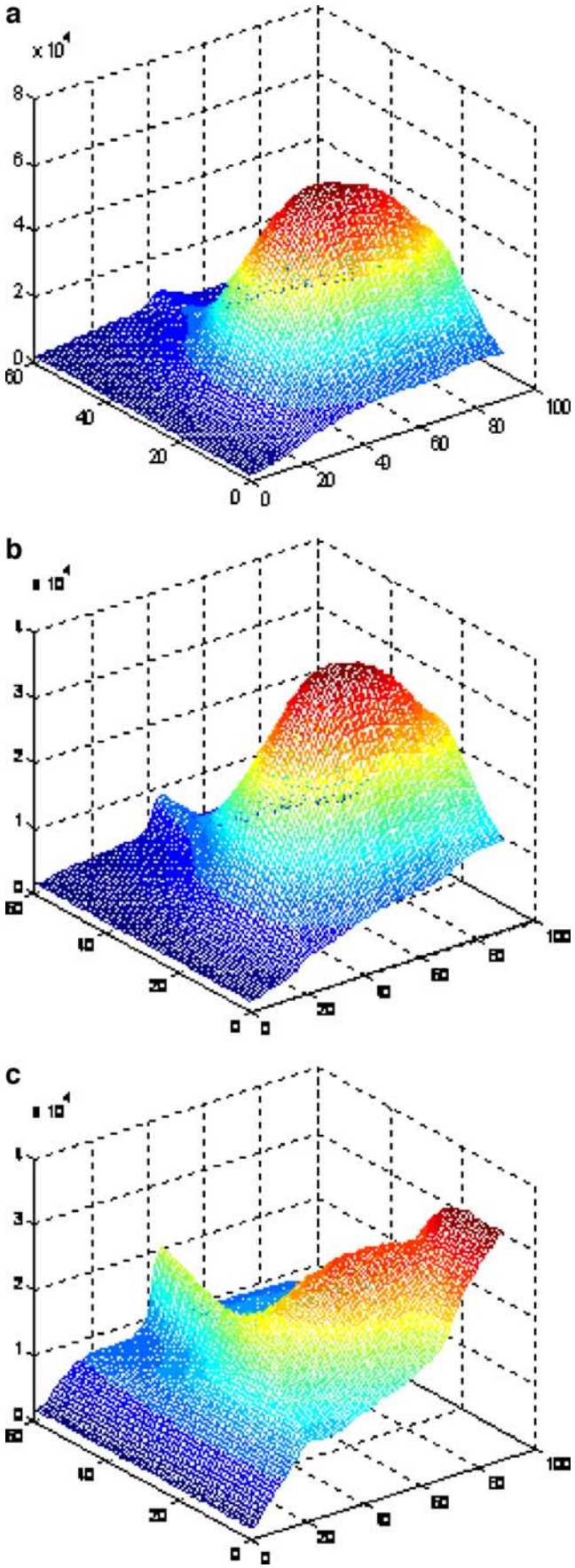

Fig. 5 EEM of QD_{550} in the presence of Pb(II): 0 μM (**a**), 3.5 μM (**b**) and 9.4 μM (**c**)

The analysis of Fig. 5 clearly shows that the fluorescence band quenches when Pb(II) is present and that several background bands can easily be detected, particularly when Pb(II) is in relatively excess (Fig. 5c). These background signal are mainly due to scattering—the first order scatter band increases its intensity when the concentration of Pb(II) is relatively high. Consequently, these results show that EEMs of QD are a mixture of fluorescence bands and other spectral sources not necessary constant.

In order to analyse the structure of the EEM acquired as function of the Pb(II) concentration PARAFAC analysis was done using different component models (from two and up to four components). Typical values for the corcondia test (explained variance) for these three models were: two components, 100% (99.59%); three components, 46.7% (99.88%); and, four components, −5% (99.94 %). These error parameters show that the intrinsic EEM model is constituted by two or three components.

Figures 6 and 7 show typical results of the trilinear decomposition of sets of EEM of QD_{550} collected in the presence of increasing amounts of Pb(II) ion. The comparison of the calculated excitation (Figs. 6a and 7a), emission (Figs. 6b and 7b) and quenching profiles (Fig. 6c and 7c) shows that the first component in both models is the same. The characteristics of the second component in the two-component PARAFAC model are divided into two components (second and third) in the three-component PARAFAC model.

The first component unequivocally corresponds to the QD_{550} fluorescence bands because the position of the excitation and emission bands agrees with that discussed above and the quenching profile (Fig. 6c and 7c) shows the expected decreasing trend. Also, and quite importantly, the fact that only one component corresponds to the quenching of the QD_{550} fluorescence shows that the presence of Pb(II) does not provoke any displacement or distortion of the fluorescence bands—only quenching of fluorescence is indeed observed.

The analysis of the quenching profiles of the other components show that they are almost constant until the concentration of Pb(II) becomes relatively high, when a marked increase of the intensity is observed. This result suggests that background signal of the EEM is almost constant for relatively small concentrations of Pb(II), increasing its intensity for higher concentrations of Pb(II) when scatter bands increase intensity due to colloid or insoluble species formation.

The analysis of the PARAFAC decomposition in general and the quenching profiles in particular, show that the isolation of the quenching variations due to Pb(II) from

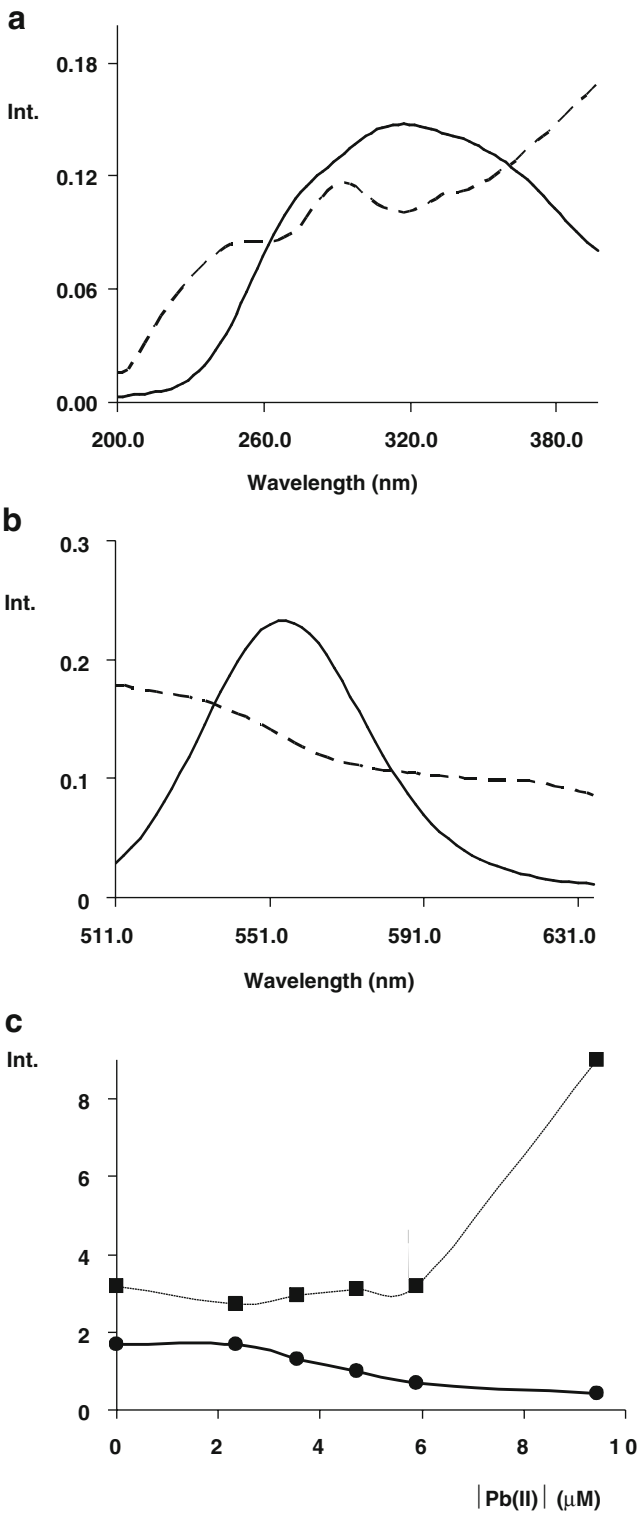

Fig. 6 Excitation (**a**) and emission (**b**) spectra and intensity profiles (**c**) calculated with a two component PARAFAC model: (*solid line*) first component; (*dashed line*) second component

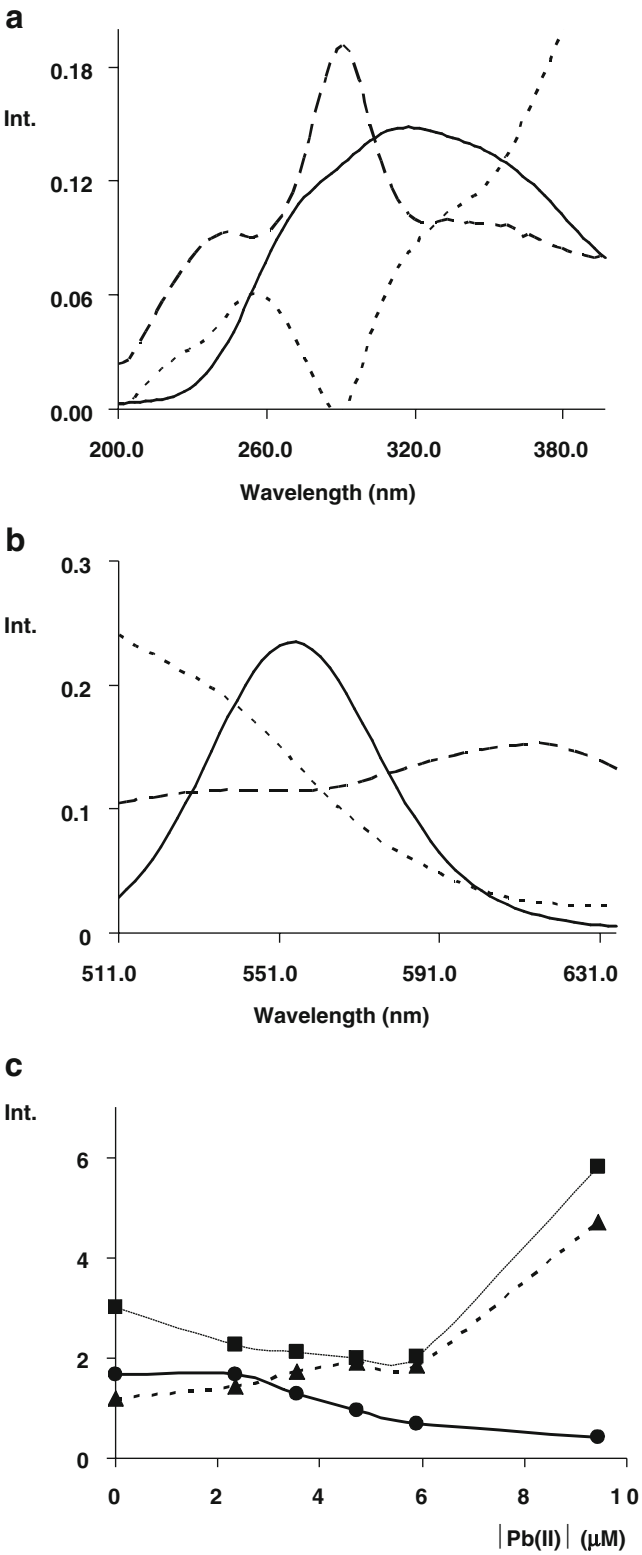

Fig. 7 Excitation (**a**) and emission (**b**) spectra and intensity profiles (**c**) calculated with a three component PARAFAC model: (*solid line*) first component; (*dashed line*) second component; (*dotted line*) third component

other background spectral signals was fully achieved and purer information about the quenching phenomena was obtained.

Stern–Volmer plots of the quenching profiles show strong upward curvature which might suggest the existence of both dynamic and static quenching [23]. However the justification for the deviation from linearity of the Stern–Volmer plot is probably much more complex than the existence of the two quenching mechanisms because each QD is capped by many GSH molecules and when one ligand complexes one Pb(II) ion it affects differently the fluorescence of the QD. Also, QD have a heterogeneous size which corresponds to a different number of GSH molecules per QD. Nevertheless, using the smaller Pb(II) concentration range, a rough estimation of a Stern–Volmer constant of 7×10^5 M^{-1} was obtained from the slope of the approximately linear plot. This order of magnitude is compatible with the formation of a quite stable complex (static quenching) between the GSH capping ligands and Pb(II) ions.

Two quenching mechanisms have been proposed to explain the decrease of fluorescence intensity of QD when metal ions are present: (1) competitive ligand (capping molecule) binding between the QD core and the metal ions present in the solution and when the ligand was displaced from the surface of the QD created imperfection on the QD surface [11]; (2) the complexation of metal ions by surface ligands of QD provokes a charge transfer process on the surface of the QD [18]. This work showed that the effect of the presence of Pb(II) on the fluorescence of QD is similar to the reversible effect of the increasing the concentration of H^+ (decreasing the pH), i.e. quenching the fluorescence. However, in the case of the pH, a shift of the emission wavelength towards longer wavelengths is also observed. This variation shows that the neutralization of the GHS capping molecules influence the QD bandgap energy as a result of the decreasing negative charge accumulation on the QD surface as the pH is decrease. The shift towards longer wavelengths and quenching of the fluorescence correspond to the decreasing confinement of the charge carriers in the QD. The complexation of Pb(II) by the ionized GSH capping molecules also provokes the decrease of the negative charge accumulation on the QD surface and consequently the decreasing confinement of the charge carriers in the QD. However, in this work there are no experimental results that could support either of the two proposed mechanisms.

The fact that the quenching provoked on the QD_{600} is much less significative than for the QD_{550} can be explained by either of the two mechanisms. Indeed, because the number of capping molecules that exists in QD_{600} is higher than in QD_{550}, the charge neutralization or the displacement of GSH molecules from the surface of QD provokes a relatively smaller effect on the fluorescence of QD.

Conclusions

GSH capped CdTe QD (with a size of about 30 nm) are easily synthesized and its steady state fluorescence properties are quite sensible to the pH of the aqueous solution and its fluorescence intensity is quenched by micromolar concentrations of Pb(II) ion.

The presence of Pb(II) does not provoke displacement nor distortions of the EEM of the QD which allows the extraction of pure quenching profiles using PARAFAC. Besides the estimation of the excitation and emission spectra this spectral decomposition method allows robust estimations of the quenching profiles. This information is particularly relevant for quantitative analytical applications of QD because the predictions of the concentrations of the quenchers are primarily based on the quality of the quenching profiles.

The results presented in this work showed that PARAFAC is a suitable method to obtain robust analytical information because the full EEM data points can be used, instead of one or a small number of fluorescence intensities, and due to the second order advantage the estimation of the quenching profiles is obtained with any background signals interference.

Acknowledgements Financial support from Fundação para a Ciência e Tecnologia (Lisboa) (FSE-FEDER) (Projects PTDC/QUI/71001/2006 and POCTI/QUI/44614/2002) is acknowledged.

References

1. Wu XY, Liu HJ, Liu JQ, Haley KN, Treadway JA, Larson JP, Ge NF, Peale F, Bruchez MP (2003) Immunofluorescent labeling of cancer markers Her2 and other cellular targets with semiconductor quantum dots. Nat Biotechnol 21:41–46
2. Jaiswal JK, Simon SM (2004) Potentials and pitfalls of fluorescent quantum dots for biological imaging. Trends Cell Biol 14:497–504
3. Gao X, Yang L, Petros JA, Marshall FF, Simons JW, Nie S (2005) *In vivo* molecular and cellular imaging with quantum dots. Curr Opin Biotechnol 16:63–72
4. Gerion D, Pinaud F, Williams SC, Parak WJ, Zanchet D, Weiss S, Alivisatos AP (2001) Synthesis and properties of biocompatible water-soluble silica-coated CdSe/ZnS semiconductor quantum dots. J Phys Chem B 105:8861–8871
5. Murphy CJ (2002) Optical sensing with quantum dots. Anal Chem 74:520A–526A
6. Green M, Harwood H, Barrowman C, Rahman P, Eggeman A, Festry F, Dobson P, Ng T (2007) A facile route to CdTe nanoparticles and their use in bio-labelling. J Mater Chem 17: 1989–1994
7. Barglik-Chory C, Remenyi C, Strohm H, Muller G (2004) Adjustment of the band gap energies of biostabilized CdS nanoparticles by application of statistical design of experiments. J Phys Chem B 108:7637–7640
8. Bãumle M, Stanou D, Segura JM, Hovius R, Vogel H (2004) Highly fluorescent streptavidil-coated CdSe nanoparticles: prepa-

ration in water, characterization, and micropatterning. Langmuir 20:3828–3831
9. Zheng Y, Gao S, Ying JY (2007) Synthesis and cell-imaging applications of glutathione-capped CdTe quantum dots. Adv Mater 19:376–380
10. Zheng Y, Yang Z, Ying JY (2007) Aqueous synthesis of glutathione-capped ZnSe and $Zn_{1-x}Cd_xSe$ alloyed quantum dots. Adv Mater 19:1475–1479
11. Ali EM, Zheng Y, Yu H, Ying JY (2007) Ultrasensitive Pb^{2+} detection by glutathione-capped quantum dots. Anal Chem 79: 9452–9458
12. Tortiglione C, Quarta A, Tino A, Manna L, Cingolani R, Pellegrino T (2007) Synthesis and biological assay of GSH functionalized fluorescent quantum dots for staining hydra vulgaris. Bioconjug Chem 18:829–835
13. Chen Y, Rosenzweig Z (2002) Luminescent CdS quantum dots as selective ion probes. Anal Chem 74:5132–5138
14. Jin WJ, Costa-Fernández JM, Pereiro R, Sanz-Mendel A (2004) Surface-modified CdSe quantum dots as luminescent probes for cyanide determination. Anal Chim Acta 522:1–8
15. Liang JG, Ai XP, He ZK, Pang DW (2004) Functionalized CdSe quantum dots as selective silver ion chemodosimeter. Analyst 129:19–622
16. Chen JL, Zhu CQ (2005) Functionalized cadmium sulfide quantum dots as fluorescence probe for silver ion determination. Anal Chim Acta 546:147–153
17. Fernández-Arguelles MT, Jin WJ, Costa-Fernández JM, Pereiro R, Sanz-Medel A (2005) Surface-modified CdSe quantum dots for the sensitive and selective determination of Cu(II) in aqueous solutions by luminescence measurements. Anal Chim Acta 549: 20–25
18. Chen J, Gao Y, Xu Z, Wu G, Chen Y, Zhu C (2006) A novel fluorescence array for mercury(II) ion in aqueous solution with functionalized cadmium selenide nanoclusters. Anal Chim Acta 577:77–84
19. Wang JH, Wang HQ, Zhang HL, Li XQ, Hua XF, Cao YC, Huang ZL, Zhao YD (2007) Purification of denatured bovine serum albumin coated CdTe quantum dots for sensitive detection of silver(I) ions. Anal Bioanal Chem 388:969–974
20. Diao XL, Xia YS, Zhang TL, Li Y, Zhu CQ (2007) Fluorescence-detecting cationic surfactants using luminescence CdTe quantum dots as probes. Anal Bioanal Chem 388:1191–1197
21. Wang YQ, Ye C, Zhu ZH, Hu YZ (2008) Cadmium tellurium quantum dots as pH-sensitive probes for tiopronin determination. Anal Chim Acta 610:50–56
22. Chen J, Zheng A, Gao Y, He C, Wu G, Chen Y, Kai X, Zhu C (2007) Functionalized CdS quantum dots-based luminescence probe for detection of heavy metal and transition metal ions in aqueous solution. Spectrochim Acta A Mol Biomol Spectrosc 69:1044–1052. doi:10.1016/j.saa.2007.06.021
23. Lakowicz JR (2006) Principles of fluorescence spectroscopy, 3rd edn. Springer, New York
24. Booksh KS, Kowalski BR (1994) Theory of analytical chemistry. Anal Chem 66:782A–765A
25. Harshman RA (1970) Foundations of the PARAFAC procedure: models and conditions for an "explanatory" multi-mode factor analysis. UCLA Working Papers Phonetics 16:1–84
26. Leurgans S, Ross R (1992) Multilinear models: applications in spectroscopy. Stat Sci 7:289–310
27. Bro R (1997) PARAFAC. Tutorial and applications. Chemom Intell Lab Syst 38:149–171
28. Appellof CJ, Davidson ER (1981) Strategies for analysing data from video fluorometric monitoring of liquid chromatographic effluents. Anal Chem 53:2053–2056
29. Burdick DS, Tu XM, McGown LB, Millican DW (1990) Resolution of multicomponent fluorescent mixtures by analysis of the excitation–emission–frequency array. J Chemom 4:15–28
30. Sanchez E, Kowalski BR (1990) Tensorial resolution: a direct trilinear decomposition. J Chemom 4:29–45
31. Smilde AK, Doornbos DA (1991) Three-way methods for the calibration of chromatographic systems: comparing PARAFAC and three-way PLS. J Chemom 5:345–360
32. Smilde AK (1992) Three-way analyses problems and prospects. Chemom Intell Lab Syst 15:143–157
33. Zeng Y, Hopke PK (1992) A new receptor model: a direct trilinear decomposition followed by a matrix reconstruction. J Chemom 6:65–83
34. Esteves da Silva JCG, Novais SAG (1998) Trilinear PARAFAC decomposition of synchronous fluorescence spectra of mixtures of the major metabolites of acetylsalicylic acid. Analyst 123:2067–2070
35. Esteves da Silva JCG, Leitão JMM, Costa FS, Ribeiro JLA (2002) Detection of verapamil drug by fluorescence and trilinear decomposition techniques. Anal Chim Acta 453:105–115
36. Rodríguez-Cuesta MJ, Boqué R, Rius FX, Zamora DP, Galera MM, Frenich AG (2003) Determination of carbendazim, fuberidazole and thiabendazole by three-dimensional excitation–emission matrix fluorescence and parallel factor analysis. Anal Chim Acta 491:47–56
37. Olivieri AC, Arancibia JA, Muñoz de la Peña A, Durán-Merás I, Mansilla AE (2004) Second-Order advantage achieved with four-way fluorescence excitation–emission–kinetic data processed by parallel factor analysis and trilinear least-squares. Determination of methotrexate and leucovorin in human urine. Anal Chem 76:5657–5666
38. Rinnan Å, Andersen CM (2005) Handling of first order Rayleigh scatter in PARAFAC modelling of fluorescence excitation–emission data. Chemom Intell Lab Syst 76:91–99
39. Nahorniak ML, Cooper GA, Kim Y, Booksh KS (2005) Three-and four-way parallel factor (PARAFAC) analysis of photochemically induced excitation–emission kinetic fluorescence spectra. Analyst 130:85–93
40. Christensen J, Becker EM, Frederiksen CS (2005) Fluorescence spectroscopy and PARAFAC in the analysis of yogurt. Chemom Intell Lab Syst 75:201–208
41. Holbrook RD, Yen JH, Grizzard TJ (2006) Characterizing natural organic material from the Occoquan Watershed (Northern Virginia, US) using fluorescence spectroscopy and PARAFAC. Sci Total Environ 361:249–266
42. Leitão JMM, Esteves da Silva JCG, Girónc AJ, Muñoz de la Peña A (2008) Optimization of Verapamil drug analysis by Excitation–Emission fluorescence in combination with second-order multivariate calibration. J Fluoresc (in press)
43. Bro R, Kiers HAL (2003) A new efficient method to determining the number of components in PARAFAC models. J Chemom 17:274–286
44. Huang J, Sooklal K, Murphy CJ, Ploehn HJ (1999) Polyamine-quantum dots nanocomposites: linear versus starburst stabilizer architectures. Chem Mater 11:595–3601
45. Li L, Qian H, Fang N, Ren J (2006) Significant enhancement of the quantum yield of CdTe nanocrystals synthesized in aqueous phase by controlling the pH and concentration of precursors solutions. J Luminesc 116:59–66
46. Deng Z, Zhang Y, Yue J, Tang F, Wei Q (2007) Green and orange quantum dots as effective pH-sensitive fluorescent probes for dual simultaneous and independent detection of viruses. J Phys Chem B 111:12024–12031
47. Skoog DA, West DM, Holler FJ (1996) Fundamentals of analytical chemistry, 7th edn. Saunders College, Fort Worth